



Synthesis and effect of electrode heat-treatment on the superior lithium storage performance of Co₃O₄ nanoparticles



Jingjing Zhang, Tao Huang*, Aishui Yu*

Department of Chemistry, Shanghai Key Laboratory of Molecular Catalysis and Innovative Materials, Institute of New Energy, Lab of Advanced Materials, Collaborative Innovation Center of Chemistry for Energy Materials, Fudan University, Shanghai 200438, China

HIGHLIGHTS

- Single-crystal Co₃O₄ nanoparticles were prepared with the assist of lysine.
- The initial irreversible loss is largely decreased after binder heat-treatment.
- The cycling performance is greatly improved after binder heat-treatment.
- For Co₃O₄ electrodes, the optimal heat-treatment temperature is 200 °C.
- The Co₃O₄ electrodes have a high capacity of 1000 mA h g⁻¹ at 170th cycle.

ARTICLE INFO

Article history:

Received 31 July 2014

Received in revised form

19 September 2014

Accepted 22 September 2014

Available online 26 September 2014

Keywords:

Cobalt oxide

Nanoparticle

Binder

Heat treatment

Lithium-ion battery

Anode material

ABSTRACT

Single-crystal Co₃O₄ nanoparticles are produced via a novel lysine-assisted hydrothermal process. When used as anode materials for lithium-ion batteries, a heat-treatment process is first introduced to decrease the initial irreversible loss and enhance the cyclability of Co₃O₄ nanoparticle-based electrodes using a polyvinylidene fluoride (PVDF) binder. Heat-treated electrodes exhibit improved lithium storage properties relative to those that are unheated. In particular, Co₃O₄ electrodes heated at 200 °C have the highest capacity and best reversibility: 1000 mA h g⁻¹ with 95.2% capacity retention after 170 cycles at a current density of 100 mA g⁻¹. Even when cycled at a high rate of 1000 mA g⁻¹, a reversible capacity up to 600 mA h g⁻¹ can still be maintained after 500 cycles. These improvements are explained based on the results from thermal analysis, transmission electron microscopy, scanning electron microscopy, nano-scratch tests, and electrochemical impedance spectroscopy measurements. Heat treatment not only improves binder distribution and adhesion to both Co₃O₄ particles and the substrate but also ensures high interfacial conductivity and keeps the active material particles and carbon black electrically connected, thereby leading to superior electrochemical performance. The results suggest that the heat-treated Co₃O₄ electrode may be a promising anode for next-generation lithium-ion batteries.

© 2014 Elsevier B.V. All rights reserved.

1. Introduction

Rechargeable lithium-ion batteries (LIBs) have attracted considerable attention as one of the most promising and viable green options for energy storage. Conventional graphitic carbons used as anode materials in commercial LIBs exhibit poor rate performance induced by a low Li diffusion coefficient [1]. Meanwhile, because of the low operating voltage, dendritic lithium is easily formed on the surface of graphite, which causes serious safety issues and poor cycle life [2–5]. Therefore, extensive effort has been

devoted to developing new anode materials with higher capacity and better safety to meet the growing demands of high-performance batteries for electric vehicles and energy storage systems. Co₃O₄ has been implemented as a promising alternative anode material because of its high theoretical capacity (890 mA h g⁻¹) and safety [6,7]. However, a large specific volume change commonly occurs in the host matrix during the cycling process, which leads to the pulverization of the electrodes and rapid capacity decay and presents a huge challenge for practical applications [8,9]. To circumvent these obstacles, nanosized Co₃O₄ materials have been extensively investigated due to their reduced lithium diffusion length, which results in faster charge/discharge and the ability to accommodate strain through volume expansion [10,11]. Recently, various nanostructured Co₃O₄, including

* Corresponding authors. Tel./fax: +86 21 51630320.

E-mail addresses: huangt@fudan.edu.cn (T. Huang), asyu@fudan.edu.cn (A. Yu).

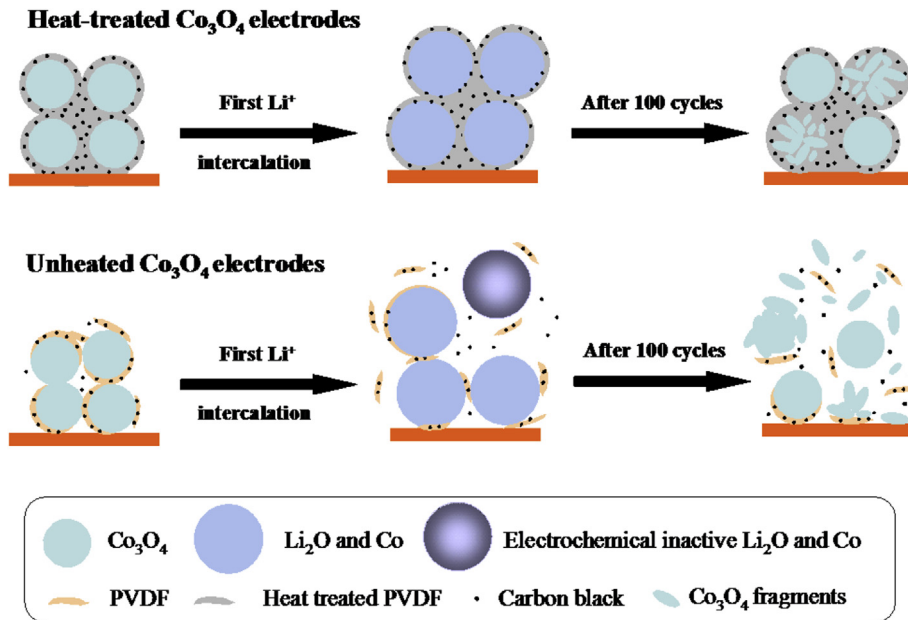


Fig. 1. Schematic comparison of unheated PVDF-based Co_3O_4 electrodes and those heated at 200 °C.

nanotubes [12], nanowires [9,13] and nanoneedles [14], have been reported to have high lithium storage capacities. Manthiram et al. reported hollow Co_3O_4 nanospheres that could deliver a reversible capacity of 786 mA h g⁻¹ after 50 cycles [15]. Wang et al. synthesized Co_3O_4 nanobelt arrays that demonstrated a reversible capacity of 770 mA h g⁻¹ over 25 cycles [16]. However, the outcomes of these studies show limited improvement over long-term cycling. Meanwhile, Co_3O_4 nanostructures with excellent long cycling stability (over 150 cycles) are not commonly reported. Although the

optimization of nanostructured materials contributes significantly to overcoming the problem of capacity-fading due to particle cracking, capacity-fading caused by huge volume change remains a major challenge for composite electrodes because of the significant motions of particles within composite electrodes during cycling [17]. The connection between the electrode binder and active material particles is broken because the particles undergoing a large volume change tend to move, collide, and shuffle past one another as the electrode cycles. Therefore, the electrode binder, not the

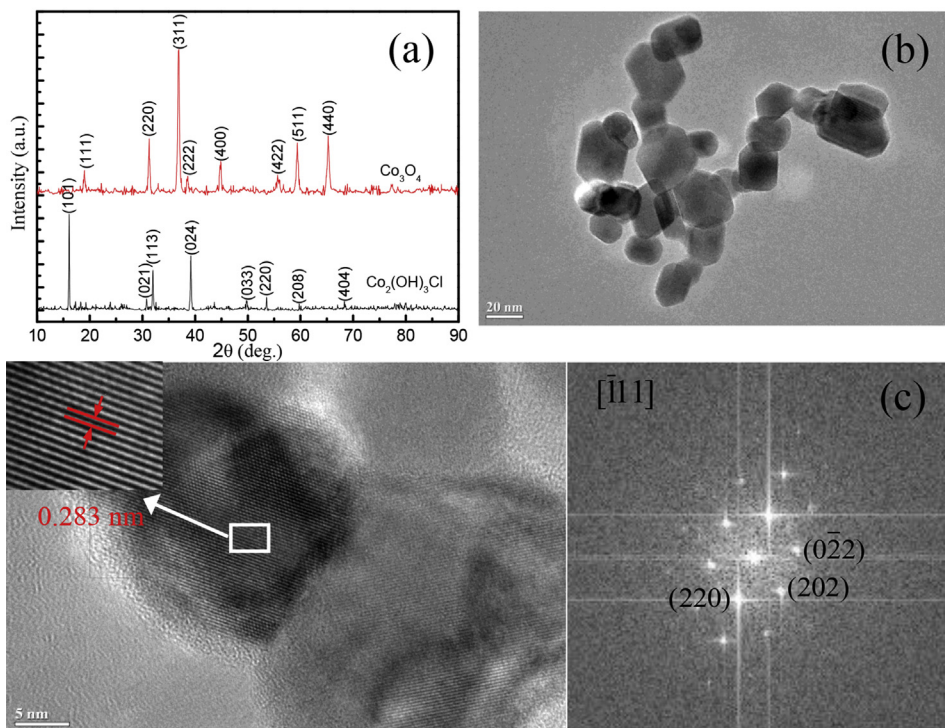


Fig. 2. (a) XRD patterns of $\text{Co}_2(\text{OH})_3\text{Cl}$ precursor and Co_3O_4 nanoparticles; (b) TEM image, (c) HRTEM image and the corresponding FFT pattern of Co_3O_4 nanoparticles.

nano-particles, are responsible for the capacity fade, and it fails to adhere to the particles during the large volume expansion, resulting in electrical isolation and consequent capacity fade [18]. Meanwhile, relatively large initial irreversible loss is another major drawback for Co_3O_4 materials. Initial irreversible capacity is usually caused by the following: some electrons and lithium ions are consumed during the irreversible formation of the SEI on the electrode surface; some lithium ions are trapped in the electrode; and a huge volume expansion of the electrode during the first lithiation makes some of the particles lose their electric contact. The third possibility is directly linked to the performance of the binder. Thus, we suggest that the polymeric binder, which not only holds the active materials and carbon black together but also ensures their attachment to the substrate, is also very important in the performance of Co_3O_4 electrodes [19].

Recent studies have suggested that normal PVDF binders may not be suitable for composite electrodes based on alloys and metal oxides that undergo a huge volume change during charge/discharge [20–22]. However, until now, little work has focused on improving the conventional PVDF binder-based systems. In this study, we present the first synthesis of single-crystal Co_3O_4 nano-particles with lysine as a hydrolysis-controlling agent. Meanwhile, heat treatment is first introduced to Co_3O_4 nanoparticle-based electrodes using a traditional PVDF binder. Remarkably, the present study shows that the heat-treatment process and temperature strongly influence the electrochemical performance of Co_3O_4 electrodes using a PVDF binder. Combined with other tests, we believe that during heat treatment, the PVDF binder, which is filled with carbon black, forms a more uniform distribution on the surface of the active material particles and the substrate, which results in superior adhesion to the active materials and to the substrate, improved electrical contact between active materials and carbon black, and superior electrochemical performance. The basis for our study is illustrated schematically in Fig. 1.

2. Experimental

2.1. Preparation of Co_3O_4 nanoparticles

All reagents purchased from Shanghai Sinopharm Chemical Reagent Co., Ltd. are analytically pure and used as-received without further purification. In a typical synthesis [23], 2 g lysine and

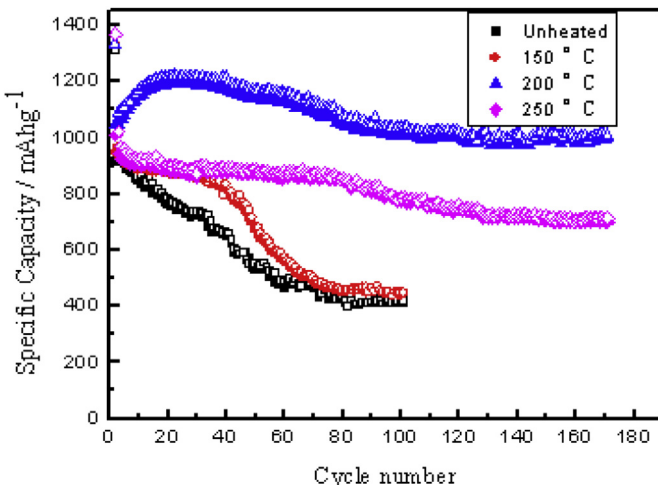


Fig. 3. Cycling performances of unheated PVDF-based Co_3O_4 electrodes and those heated at 150, 200 and 250 °C at 100 mA g^{-1} in the voltage range of 0.01–3.0 V (open-discharge, filled-charge).

1.3568 g $\text{CoCl}_2 \cdot 6\text{H}_2\text{O}$ were dissolved in 50 mL deionized water. The resulting solution was transferred to a Teflon-lined autoclave and maintained at 100 °C for 24 h. After reaction, the autoclave was cooled to room temperature naturally. The products were obtained by centrifuging and sequentially washing with water and ethanol several times, followed by drying in a vacuum oven at 60 °C for 12 h. Then, the precursor was heated in air at 500 °C for 6 h to yield Co_3O_4 .

2.2. Characterization and electrochemical measurements

The crystalline structure and morphology of the nanoparticles were characterized by X-ray diffraction (XRD, Bruker D8 Advance, $\text{CuK}\alpha$ radiation, 1.5406 Å) and transmission electron microscopy (TEM, JEM-2100F). The effects of annealing were examined with a thermogravimetric and differential thermal apparatus (TG/DTA) (DTG-60H, Shimadz) and scanning electron microscopy (SEM, JEOL JSM-6390). Nanoscratch tests were conducted with a nanoscratch tester (CSM Instruments, Switzerland) using a Rockwell indenter (conical, die angle 90°, tip radius 10 µm). A pre-scan procedure with a load of 1 mN was first conducted. The tip was then pushed into the sample with increasing load from 1 mN to the preset maximum load while being moved with a constant velocity to attain a 0.05-mm scratch length within 30 s.

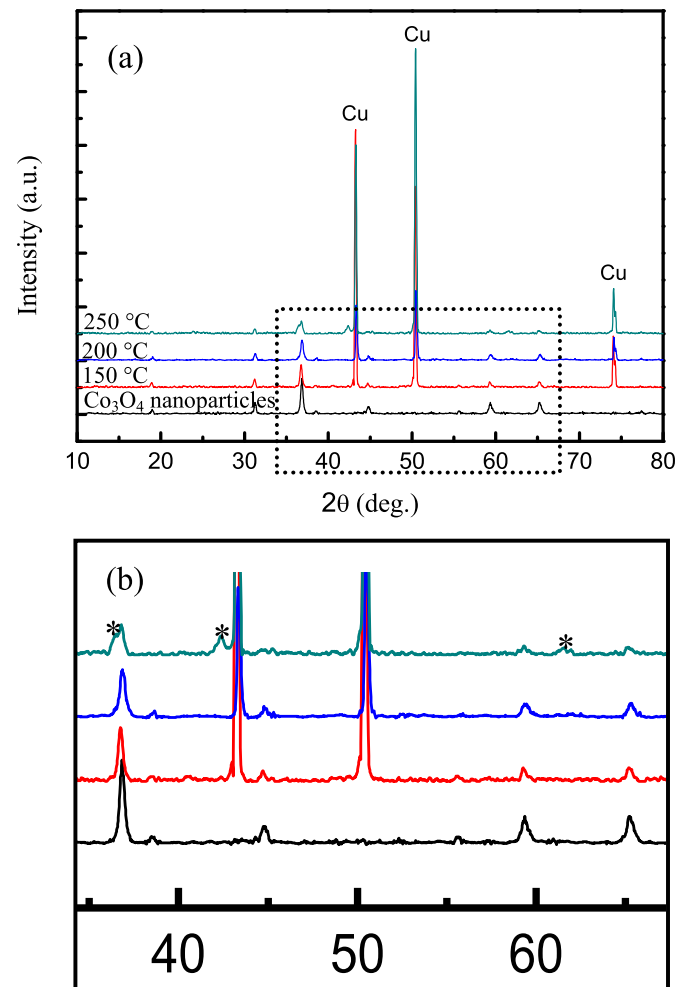


Fig. 4. (a) XRD patterns of the obtained materials: Co_3O_4 nanoparticles and PVDF-based Co_3O_4 electrodes heated at 150, 200 and 250 °C; and (b) an enlargement of the black-framed region in (a).

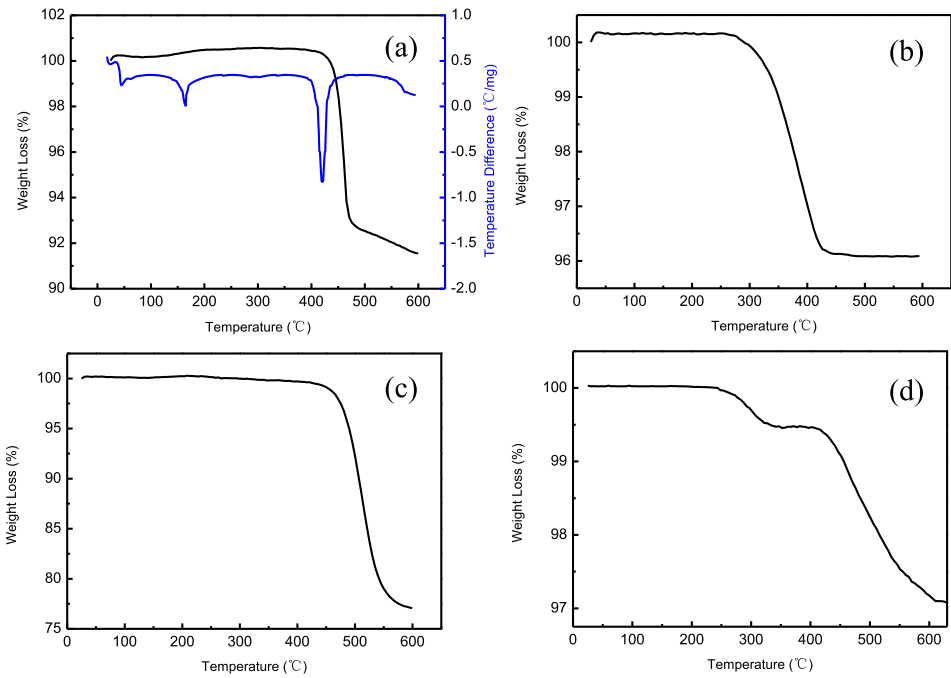


Fig. 5. (a) TGA and DTA of PVDF film; (b) TGA of Co_3O_4 and PVDF film; (c) TGA of Co_3O_4 and Super P film; and (d) TGA of Co_3O_4 , Super P and PVDF film.

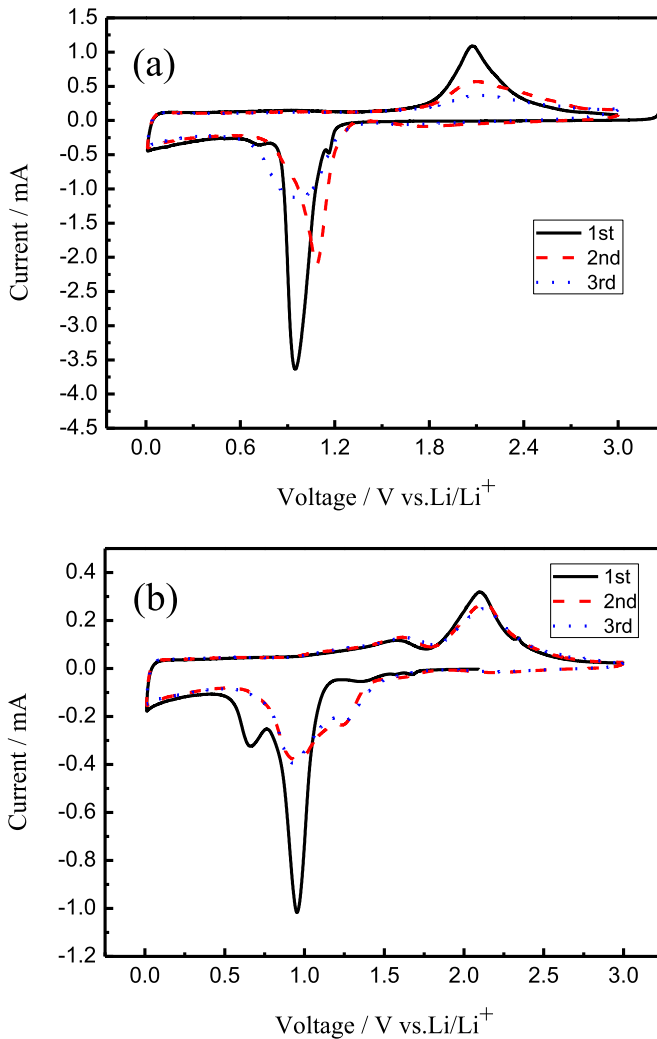


Fig. 6. Cyclic voltammograms of PVDF-based Co_3O_4 electrodes heated at (a) 200 and (b) 250 °C from the first cycle to the third cycle at a scan rate of 0.1 mV s⁻¹ in the voltage range of 0.01–3.0 V.

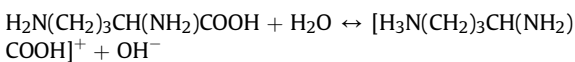
The surface profile was recorded by a depth sensor. After the tip was removed, a post-scan with a load of 1 mN was performed to determine the residual depth of the scratch. An optical microscope was employed to observe the appearance of scratch tracks. The critical normal loads for interface delamination were then obtained. The maximum load in the scratch tests for acquiring a critical load was set at 300 mN for unheated PVDF-based Co_3O_4 electrodes and 1000 mN for PVDF-based Co_3O_4 electrodes heated at 200 °C. The bending ability of the electrodes was tested in a modified condition using electron universal testing machine (CMT4104). An electrode of 10 mm wide and 0.03 mm thick was put on the machine holder with a span length of 14 mm. Then a load was pressed against the electrode with a speed of 10 mm min⁻¹ to investigate the coating stability and the recover capability of unheated PVDF-based Co_3O_4 electrodes and PVDF-based Co_3O_4 electrodes heated at 200 °C.

Electrochemical tests were performed using a CR2016-type coin cell. An assembled coin cell was composed of lithium as the counter electrode and a working electrode consisting of 80% active material, 10% super P carbon black and 10% polyvinylidene fluoride (PVDF) made on copper foil. Coin-type cells were assembled in an argon-filled glove box (Mikarouna, Superstar 1220/750/900) with 1 M LiPF₆ solution in ethylene carbonate/diethyl carbonate (EC:DEC = 1:1, v/v) as the electrolyte and Celgard 2300 as the separator. The total mass of the active electrode material was approximately 3 mg, and the electrode surface area was 1.54 cm² (Φ 14 mm). To investigate the effect of heat-treatment, some Co_3O_4 electrodes using a PVDF binder were prepared and then heated under nitrogen flow at 150, 200, and 250 °C for 2 h.

Cyclic voltammetry (CV) measurements were performed on an Electrochemical Workstation (CH Instrument 660 A, CHI Company) at a scan rate of 0.1 mV s⁻¹ in the range of 0.01–3.0 V vs. Li/Li⁺. Galvanostatic charge–discharge tests were performed on a battery test system (Land CT2001A, Wuhan Jinnuo Electronic Co. Ltd.) at a constant current density of 100 mA g⁻¹ in the potential range of 0.01–3.0 V. Electrochemical impedance spectroscopy (EIS) measurements were conducted for fresh and post-cycling cells at open potential with an ac amplitude of 5 mV over the frequency range of 10^5 to 10^{-2} Hz (CH Instrument 660 A, CHI Company).

3. Results and discussion

The crystal structures and chemical compositions of the as-prepared materials were confirmed via XRD (Fig. 2a). The XRD pattern of the precursor synthesized by the hydrothermal reaction exhibits the (101), (021), (113), (024), (033), (220), (208) and (404) peaks of the pure $\text{Co}_2(\text{OH})_3\text{Cl}$ crystalline structure, which are consistent with the standard spectrum (JCPDS 73-2134). The pH of an amino acid depends on the amount of both amino and carboxylic acid groups in the molecular structure due to the existence of the hydrolysis process. Lysine is an amino acid with two amino groups and one carboxylic acid group, so its pH should be above 7. With the hydrolysis of lysine during the hydrothermal process, increasingly more OH^- ions are formed, and the pH value of the solution increases greatly, resulting in the formation of a $\text{Co}_2(\text{OH})_3\text{Cl}$ phase. The process can be described by the following equations:



For the sample of Co_3O_4 nanoparticles after precursor thermal decomposition, eight obvious diffraction peaks can be easily identified for the (111), (220), (311), (222), (400), (422), (511) and (440) peaks of the cubic Co_3O_4 crystalline structure according to the standard spectrum of JCPDS No. 43-1003. Using Scherrer's formula, based on the (220), (311), (400), (511) and (440) planes, the grain size of Co_3O_4 is estimated to be 30.18 nm.

TEM with Fast Fourier transform (FFT) was employed to investigate the microstructure and crystallization of the obtained Co_3O_4 materials. The TEM image in Fig. 2b suggests that the materials contain nanoparticles with diameters ranging from 20 to 40 nm,

consistent with the XRD result estimated using Scherrer's formula. The FFT pattern and HRTEM image of an individual Co_3O_4 particle taken along the [111] direction are illustrated in Fig. 2c. A clear lattice fringe with an interplanar distance of 0.283 nm coincides with the d-spacing of the (220) plane in the Co_3O_4 structure. Furthermore, the corresponding FFT spots have a regular hexagonal distribution, indicating a single-crystal characteristic.

The electrochemical properties of PVDF-based Co_3O_4 electrodes heated at different temperatures for LIBs were investigated. Fig. 3 shows the cycling performances obtained at a current density of 100 mA g^{-1} in the voltage window of 0.01–3.0 V (vs. Li/Li^+). Both unheated electrodes and those heated at 150 °C show poor cycling stability and rapid degradation, and only capacities of 410 and 440 mA h g^{-1} can be obtained after 100 cycles, respectively. For a heat-treatment temperature of 200 °C, a stable capacity as high as 1000 mA h g^{-1} can be maintained without noticeable capacity-fading after 170 cycles. Remarkably, this result is a vast improvement for Co_3O_4 nanostructures because a relatively long cycling stability with extremely high reversible capacity is rarely reported [6,7,15,16,24–27]. However, upon further increasing the heat-treatment temperature to 250 °C, the ss capacity is reduced to 700 mA h g^{-1} after 170 cycles. For electrodes heated at 200 °C, the capacities in the first 20 cycles follow a similar increasing trend as previous reports, which could be attributed to reversible lithium storage in the polymeric gel-like layer [28–30].

Fig. 3 clearly shows that heat-treatment improves the performance of PVDF-based Co_3O_4 electrodes. Compared with unheated electrodes, those heated at 200 °C have the highest capacity and best reversibility. To explore the reasons for this trend, electrode materials after heat treatment were investigated via XRD, as shown in Fig. 4. The well-distinguished peaks of Co_3O_4 are observed in the same positions for electrodes heated at both 150 and 200 °C, and no impurity is observed. However, for electrodes heated at 250 °C, an additional three peaks corresponding to CoO appear (marked by

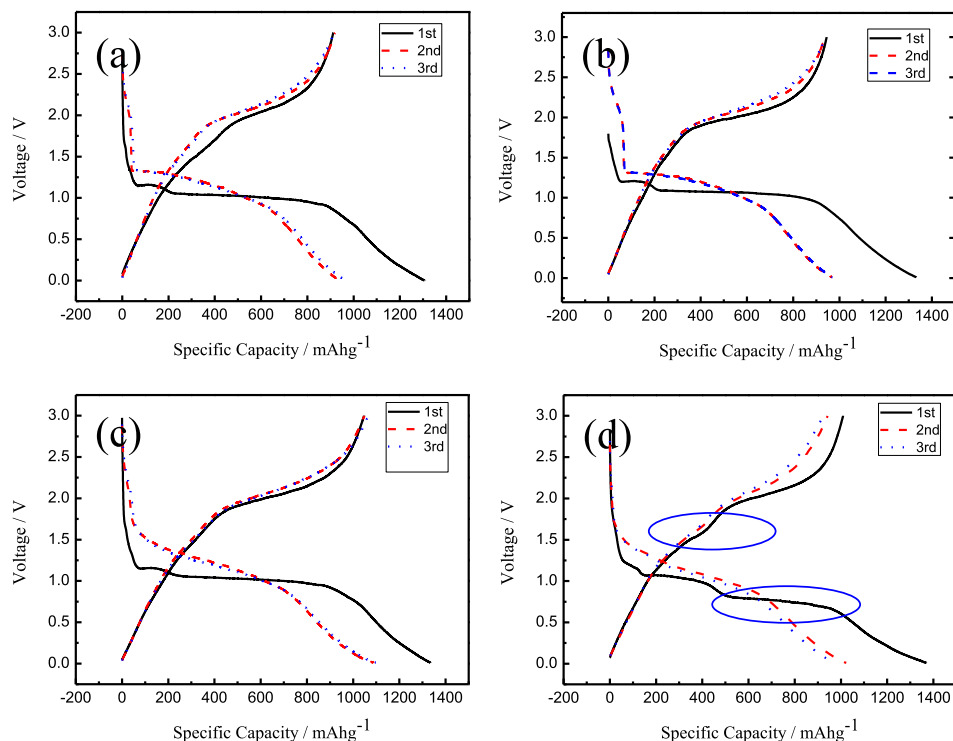


Fig. 7. Discharge/charge profiles for three cycles of (a) unheated PVDF-based Co_3O_4 electrodes and those heated at (b) 150, (c) 200 and (d) 250 °C at 100 mA g^{-1} in the voltage range of 0.01–3.0 V.

asterisks in Fig. 4 at $2\theta = 36.5, 42.4$, and 61.5° , JCPDS No. 78-0431). Phase transformations on heating are also confirmed by TGA (Fig. 5). Fig. 5a shows TGA and DTA results of the PVDF film. There is an endothermic peak around 165°C in the DTA curve, which corresponds to the melting point of the PVDF polymer. In addition, the TGA results show the onset temperature of PVDF decomposition at approximately 420°C , which corresponds to the sharp endothermic peak after 420°C in the DTA profile. Therefore, it is speculated that during heat treatment at temperatures of >165 and $<420^\circ\text{C}$, the PVDF film melts, and the long, tangled chains of PVDF move around, flatten out, and then recrystallize in the final cooling process. This heat-melt-cool process apparently allows carbon black-filled PVDF to redistribute and form a more continuous film on the active materials and substrate surface with larger cohesion. However, when Co_3O_4 is added to the composition, binder decomposition begins at a significantly reduced temperature, slightly below 250°C (Fig. 5b), which is in agreement with previous studies that show that the addition of metal oxides and nitrides to polymer compounds accelerates chain scission within the binder, reducing the decomposition temperature [31–33]. For further clarity, we also investigated the reaction between Co_3O_4 and carbon black Super P (Fig. 5c), illustrating that Co_3O_4 can be reduced by Super P until 440°C . Thus, we believe that the decomposition products of PVDF, containing ethanediol, propylene glycol, cyclohexanol and other alcohols and ketonic groups, reduce a small amount of Co_3O_4 to CoO at approximately 250°C [31], which accounts for the coexistence of Co_3O_4 and CoO after heat-treatment at 250°C . In addition, the reduction reaction and partial PVDF decomposition correspond to the weight loss at $240\text{--}340^\circ\text{C}$ of Co_3O_4 , Super P and PVDF film in Fig. 5d. And a rapid weight loss occurs above 415°C that is consistent with the complete binder breakdown and Co_3O_4 reduction. The above results suggest that the actual binder degradation temperature is dependent on the active material and that for Co_3O_4 electrodes, the optimal heat-treatment temperature is 200°C .

Fig. 6 illustrates cyclic voltammograms of PVDF-based Co_3O_4 electrodes heated at 200°C and 250°C . For electrodes heated at 200°C (Fig. 6a), there is one shoulder around 1.17 V , one strong peak at 0.95 V and two relatively weak peaks near 0.72 V and 0.01 V during the first cathodic scan. The shoulder around 1.17 V and the strong peak at 0.95 V should be attributed to the partial reduction process to $\text{Li}_x\text{Co}_3\text{O}_4$ and the further reduction to Co and Li_2O ($\text{Co}_3\text{O}_4 + x\text{Li}^+ + xe^- \rightarrow \text{Li}_x\text{Co}_3\text{O}_4$, $\text{Li}_x\text{Co}_3\text{O}_4 + (8-x)\text{Li}^+ + (8-x)e^- \leftrightarrow 3\text{Co} + 4\text{Li}_2\text{O}$), which are confirmed by the 1.15 V and 1.0 V plateaus in the first discharge curve (Fig. 7c) [34,35]. Moreover, the weak peak near 0.72 V is associated with the irreversible formation of a SEI layer [36]. The weak peak near 0.01 V , which corresponds to the continuous sloping voltage to 0.01 V in the first discharge cycle, should be ascribed to the reversible formation and decomposition of a gel-like film on the surface of oxide particles, which can lead to an extra reversible capacity in addition to the reversible reaction mechanism [31]. In the first anodic scan, only one peak appears at approximately 2.07 V , which could be related to the reversible oxidation of Co to cobalt oxide. For electrodes heated at 250°C (Fig. 6b), another pair of peaks at 0.66 V and 1.63 V occurs, corresponding to the reversible reaction of CoO with Li [36], which is consistent with the 0.73 V and 1.61 V plateaus in the first cycle in Fig. 7d, proving the coexistence of Co_3O_4 and CoO after heat-treatment at 250°C .

The charge/discharge curves of PVDF-based Co_3O_4 electrodes heated at different temperatures for three cycles obtained at a current density of 100 mA g^{-1} in the voltage window of $0.01\text{--}3.0\text{ V}$ (vs. Li/Li^+) are shown in Fig. 7. As observed in the voltage profiles, both the lack and occurrence of heat-treatment at 150°C result in

large first irreversible capacities, and the initial Coulombic efficiencies are 69.8% and 70.9% , respectively. At a heat-treatment temperature of 200°C , the initial Coulombic efficiency is significantly improved to 78.9% , and a high first-charge capacity of 1050 mA h g^{-1} is obtained. However, upon further increasing the

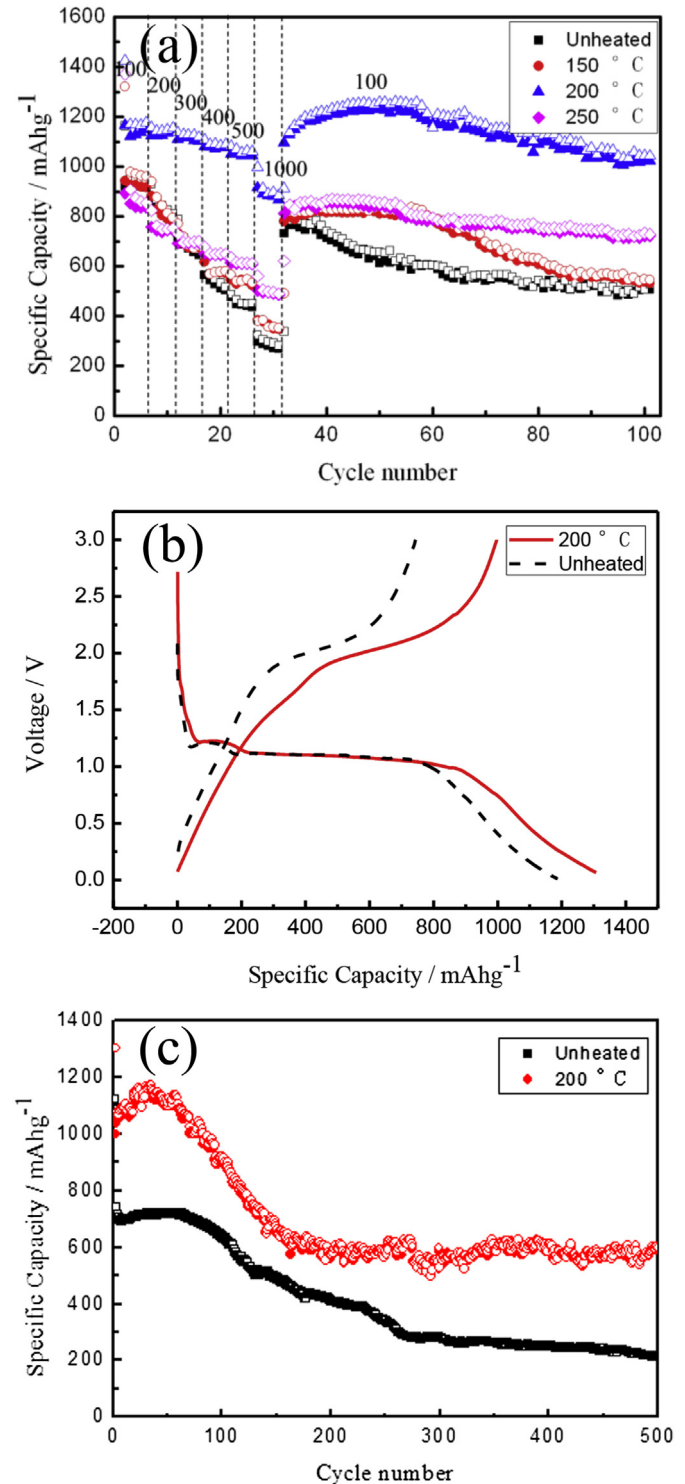


Fig. 8. (a) Rate capability ($100\text{--}1000\text{ mA g}^{-1}$) of unheated PVDF-based Co_3O_4 electrodes and those heated at different temperatures and (b) the first discharge/charge profiles at 1000 mA g^{-1} ; (c) cyclic performances at 1000 mA g^{-1} of unheated PVDF-based Co_3O_4 electrodes and those heated at 200°C in the voltage range of $0.01\text{--}3.0\text{ V}$ (open-discharge, filled-charge).

heat-treatment temperature to 250 °C, reversible capacity (1009 mA h g⁻¹) and Coulombic efficiency (73.7%) both decrease. Partial binder decomposition and the subsequent loss of cohesion may cause this phenomenon. Irreversible capacity for Co₃O₄ materials is directly linked to binder performance. During the first lithiation process, the weak connection between unheated PVDF binder and Co₃O₄ particles is partially broken because of the significant motions of Co₃O₄ particles with huge volume expansion [37]. In the following delithiation process, some of the particles

cannot electrically connect to the main body of the electrode, thereby permanently losing the corresponding capacity. As shown in Fig. 7, the irreversible capacities of the electrodes decrease after heat treatment.

The high rate performances of heat-treated Co₃O₄ electrodes are also important for applications requiring fast charging and discharging. Fig. 8a presents the rate capabilities of PVDF-based Co₃O₄ electrodes heated at different temperatures from 100 mA g⁻¹ to 1000 mA g⁻¹. Among the obtained electrodes, the one heated at

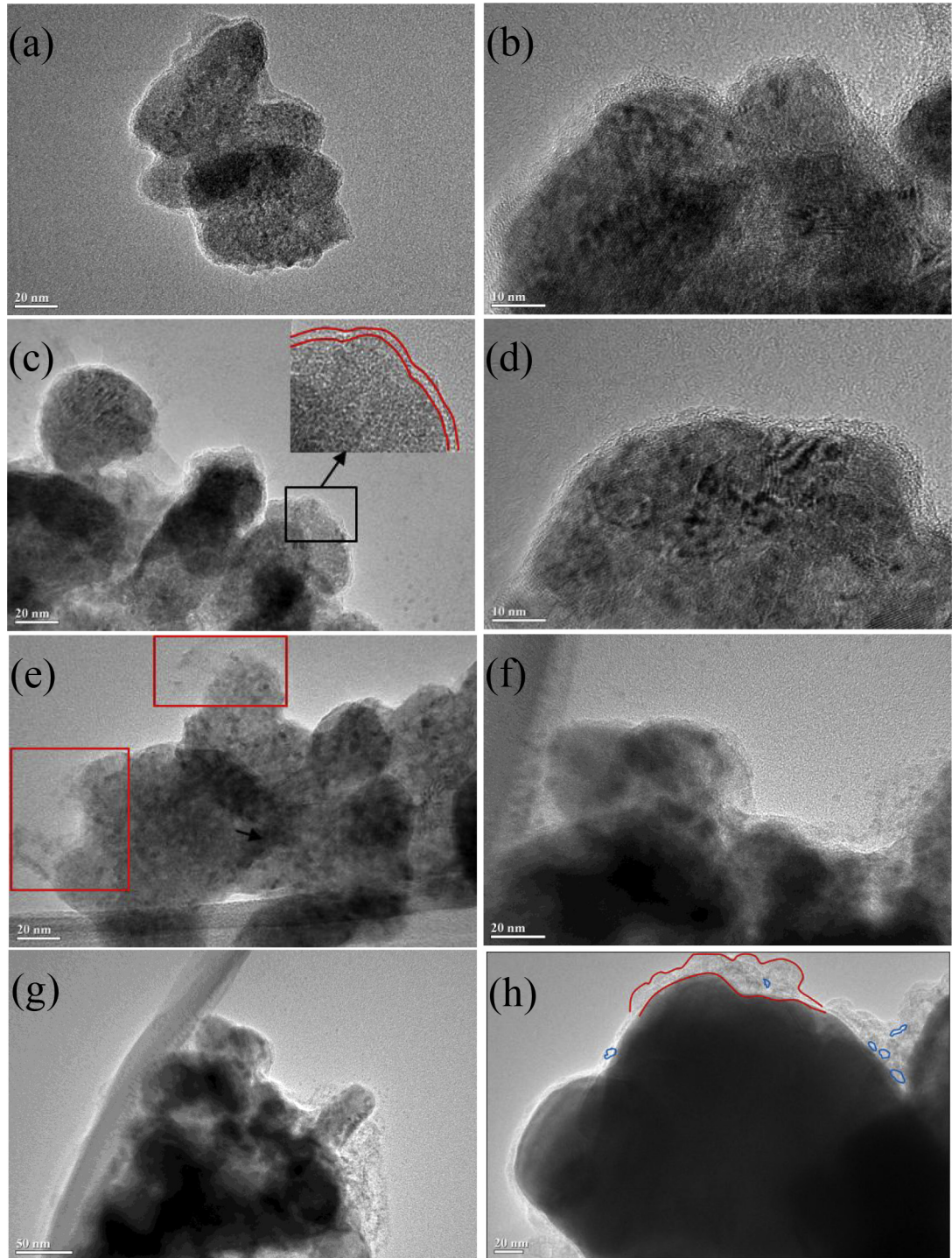


Fig. 9. TEM results of PVDF-based Co₃O₄ electrodes heated at 200 °C: (a,b) before cycling and (c,d) after cycling (100th); unheated PVDF-based Co₃O₄ electrodes: (e,f) before cycling and (g,h) after cycling (100th).

200 °C exhibits the best rate capability. No obvious fading of the charge capacity is observed during the first 5 cycles when testing at various rates. Even at a high rate of 1000 mA g⁻¹, the specific capacity remains over 870 mA h g⁻¹. More importantly, when the current density is decreased to 100 mA g⁻¹, a charge capacity of 1023 mA h g⁻¹ in the subsequent 100 cycles is still obtained, which is nearly 90% of the initial charge capacity at 100 mA g⁻¹. Notably, the capacities here are much higher than that of an unheated electrode at cycling current from 1000 mA g⁻¹ (268 mA h g⁻¹) to 100 mA g⁻¹ (508 mA h g⁻¹).

Fig. 8b displays the initial charge/discharge profiles of unheated PVDF-based Co₃O₄ electrodes and those heated at 200 °C at a higher current density of 1000 mA g⁻¹ in the potential range of 0.01–3.0 V. With increased charge/discharge rates, there is a slight drop in capacity values for electrodes heated at 200 °C, and the initial discharge and charge capacities are 1306 mA h g⁻¹ and 997 mA h g⁻¹, respectively; however, for unheated electrodes, only 1187 mA h g⁻¹ and 744 mA h g⁻¹ can be obtained. We further evaluated the long life cycle performance at a current density of 1000 mA g⁻¹, as shown in Fig. 8c. A reversible capacity of approximately 600 mA h g⁻¹ can still be obtained after 500 cycles for electrodes heated at 200 °C, and this value is only 219 mA h g⁻¹ for unheated electrodes. These electrochemical studies demonstrate

that PVDF-based Co₃O₄ electrodes heated at 200 °C exhibit superior reversible capacity, excellent cycling performance, and good rate capability.

To further explore the enhanced electrochemical performance of heat-treated PVDF-based Co₃O₄ electrodes, pre- and post-cycling (100th) TEM images were collected (Fig. 9). For the fresh electrode, a thin uniform PVDF layer of approximately 3 nm is tightly combined with Co₃O₄ crystallites after heat-treatment at 200 °C (Fig. 9a and b). More importantly, the electrode nearly retains its initial nanostructure, and Co₃O₄ nanoparticles are still covered by the PVDF layer after 100 cycles (Fig. 9c and d). By comparison, for the fresh unheated electrode, the distribution of PVDF is uneven (Fig. 9e and f). Furthermore, due to the weak cohesion between Co₃O₄ nanoparticles and PVDF, part of the PVDF layer loosely binds to the Co₃O₄ particles, and the cavities existing between layer and Co₃O₄ particles are circled; part of the layer even completely releases from the Co₃O₄ particles with a huge volume change during cycling (Fig. 9g and h). As a result, the crystallites undergo further pulverization and electrical isolation, resulting in capacity decay. Due to heat treatment, however, the PVDF polymer can flow and form a robust coating on the surface of the active material, which can then hold the Co₃O₄ nanoparticles and carbon black together during the large volume change to ensure effective electrical contact and thus lead to improved lithium storage capability.

Nanoscratch tests were employed to evaluate the adhesion strength of the electrode coatings to the Cu current collector. Fig. 10 shows the penetration depth and residual depth profiles for coatings of PVDF-based Co₃O₄ electrodes heated at 200 °C and

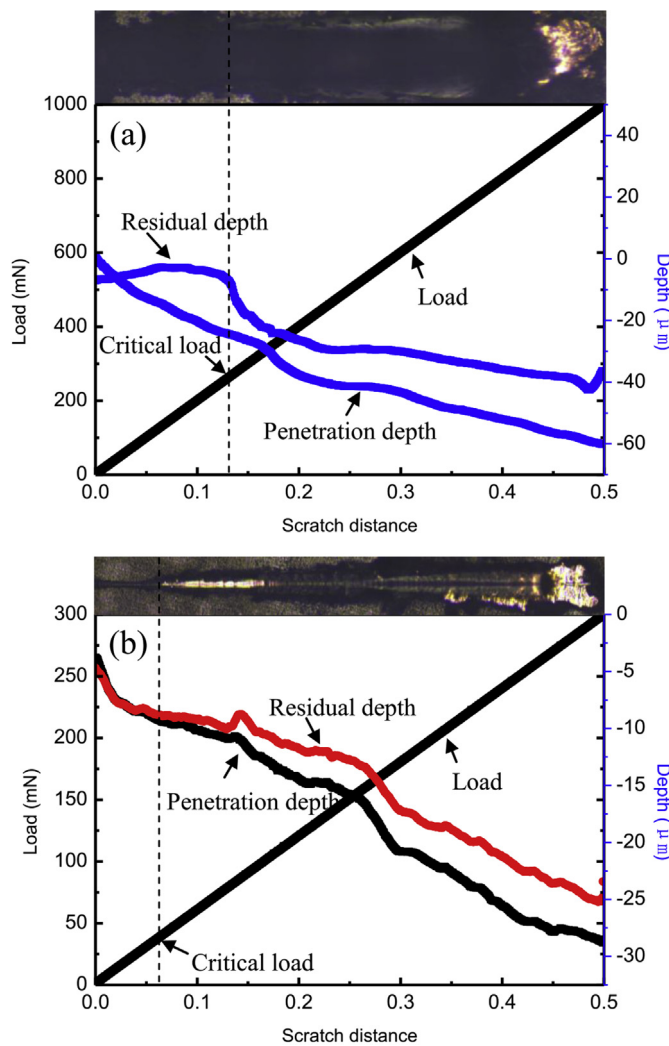


Fig. 10. Typical profiles of penetration and residual depth for (a) PVDF-based Co₃O₄ electrodes heated at 200 °C and (b) unheated PVDF-based Co₃O₄ electrodes.

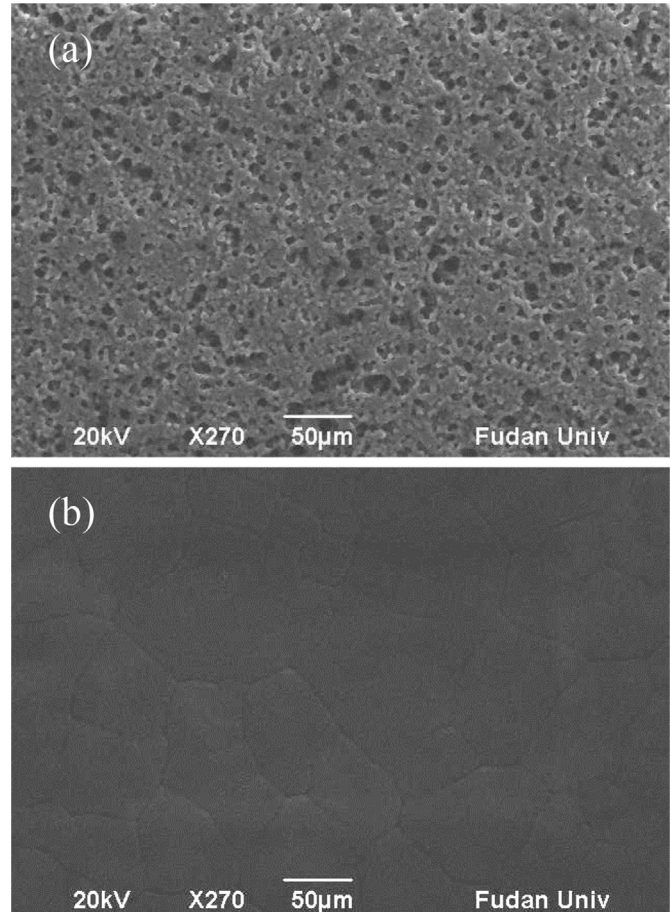


Fig. 11. SEM results of (a) unheated PVDF film and (b) PVDF film heated at 200 °C.

unheated PVDF-based Co_3O_4 electrodes in a typical scratch test with maximum loads of 1000 and 300 mN, respectively. For PVDF-based Co_3O_4 electrodes heated at 200 °C (Fig. 10a), an obvious increase in the penetration depth profile is observed at a load of 266 mN. By comparing the appearance of the film along the scratch track, 266 mN is the critical load for film failure. Below the critical load, the coating is only pressed without damage. However, when the applied load is sufficiently high, the coating buckles and chips, and the Cu current collector is exposed, which is responsible for the drastic fluctuation of the curve. For unheated PVDF-based Co_3O_4 electrodes (Fig. 10b), the critical load is much lower. Because of the poorer adhesive strength of the coating with Cu substrate, chipping of the coating is observed at a load of 41 mN. Adhesion is noticeably much improved after heat-treatment. Heat-treatment converts discrete, dense lumps of PVDF into a uniform, continuous coating on the substrate surface. Thus, the electrode coating has an area-to-area contact with the substrate instead of a dot-to-dot contact, thereby leading to better bonding with the substrate. The improved adhesion apparently contributes to an improved cycle life.

These results clearly show that heat treatment improves binder distribution and adhesion to both Co_3O_4 particles and the substrate. Actually, a freshly prepared wet Co_3O_4 electrode using a PVDF binder contains a certain amount of NMP solvent. The sequentially

drying process removes NMP, which leads to a more and more concentrated PVDF solution within the electrode. As a result, PVDF becomes more and more viscous and has a high contact angle to the Co_3O_4 surface with the generation of many pores at the end of drying process. The porous carbon black-filled PVDF with discrete and dense lumps finally forms on the surface of Co_3O_4 particles in a dried electrode. However, for heat-treated PVDF-based Co_3O_4 electrodes, the carbon black-filled PVDF polymer can flow and form a continuous coating on the surface of the active material, which is attributed to the decreased PVDF melt viscosity during heating. This situation is similar to the case of gas diffusion layers in fuel cell membrane electrode assemblies. The gas diffusion layer is generally made of carbon paper coated with Teflon (polytetrafluoroethylene) or a Teflon–carbon black mixture, followed by thermal sintering [38]. It was reported that higher sintering temperatures cause the Teflon to coat the paper fibres more thoroughly, thus allowing easier gas flow through the gas diffusion layer [38]. To further verify this assumption, the SEM images of unheated PVDF film and PVDF film heated at 200 °C were shown in Fig. 11. It can be seen that unheated PVDF film shows a porous and discrete morphology (Fig. 11a), whereas PVDF film heated at 200 °C has a much smoother, more continuous and uniform appearance (Fig. 11b). Additionally, the results here are in accordance with that of Li et al. using optical microscope [22].

Fig. 12 shows the effect of heat treatment on the electrochemical impedance of the electrodes. The experimental results are shown along with the equivalent circuits (inset). An intermediate-frequency semicircle and low-frequency tail are observed in Fig. 12a. The intermediate-frequency semicircle is related to charge transfer resistance (R_{ct}), and the low-frequency tail is associated with the Li ion diffusion process in the solid phase of the electrode. After 30 cycles, an additional high-frequency semicircle, ascribed to formation of the SEI film upon cycling, is observed in Fig. 12b. The fitted results show much decreased R_{ct} values after heat-treatment. Before charge, the R_{ct} value of the unheated PVDF-based Co_3O_4

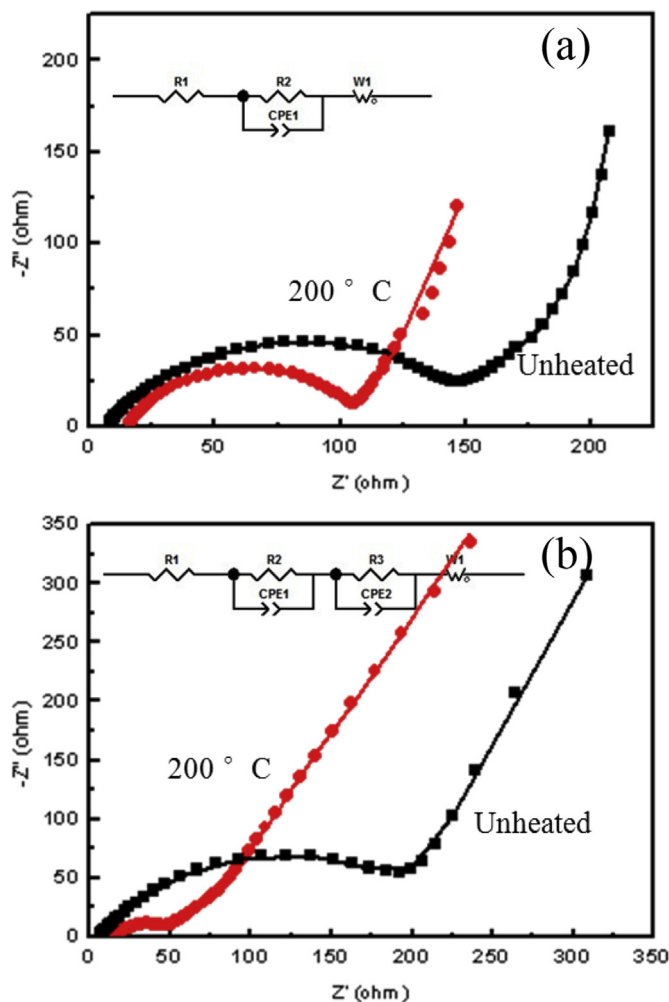


Fig. 12. Electrochemical impedance spectroscopy (EIS) and the equivalent circuits (inset) of unheated PVDF-based Co_3O_4 electrodes and those heated at 200 °C: (a) before cycling and (b) after cycling (30th) at 100 mA g⁻¹. The symbols and lines correspond to experimental and simulated data, respectively.

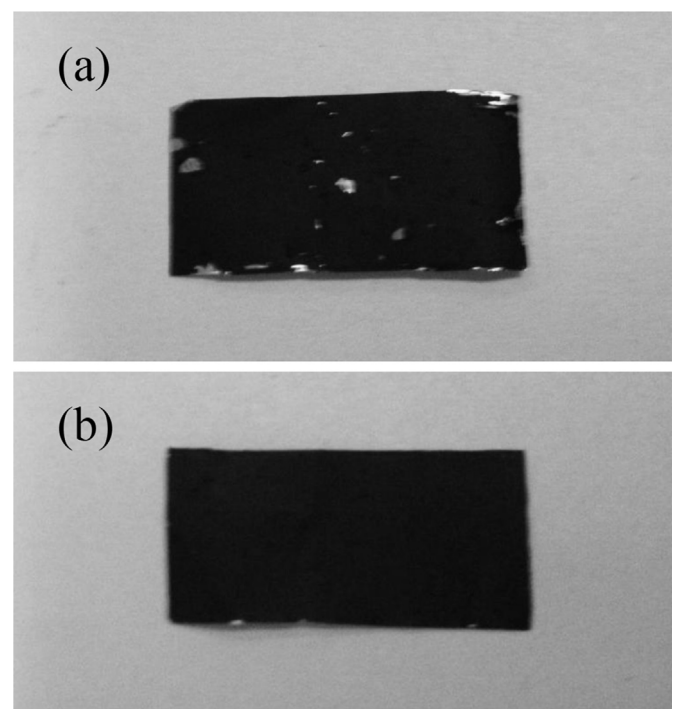


Fig. 13. Pictures of (a) unheated PVDF-based Co_3O_4 electrodes and (b) PVDF-based Co_3O_4 electrodes heated at 200 °C after bending test.

electrodes is $138.7\ \Omega$, while the PVDF-based Co_3O_4 electrodes heated at $200\ ^\circ\text{C}$ exhibit much a smaller R_{ct} value of $91.68\ \Omega$. After 30 cycles, the R_{ct} value of heat-treated samples decreases dramatically to $19.79\ \Omega$, resulting from good electrical contact and electrochemical activation [39–41], whereas the value is $173.7\ \Omega$ for unheated sample. As mentioned above, the weak connection between electrode binder and active material particles is broken during the large volume change, resulting in electrical isolation and thus much increased electronic resistance. Therefore, a better binder distribution could lead to a smaller interfacial impedance and better electrical contact between active material particles and conductive additive, leading to improved electrochemical performance.

We further investigated the bending ability of the electrodes. Under the same pressed load, partial chipping of the coating was observed for unheated PVDF-based Co_3O_4 electrodes. However, for PVDF-based Co_3O_4 electrodes heated at $200\ ^\circ\text{C}$, the coating was still tightly combined with the Cu foil and the electrodes were recovered after the bending deformation (6 mm). Obviously, the bending ability and the adhesion of the electrodes are improved after heat treatment. The pictures of unheated PVDF-based Co_3O_4 electrodes and PVDF-based Co_3O_4 electrodes heated at $200\ ^\circ\text{C}$ after bending test were shown in Fig. 13.

4. Conclusions

In summary, we have developed a facile lysine-assisted approach to fabricate Co_3O_4 nanoparticles, and the effect of PVDF binder heat treatment on the superior lithium storage performance has been systematically investigated. Electrochemical tests show that electrodes heated at $200\ ^\circ\text{C}$ have the highest capacity and best reversibility. The dramatically improved electrochemical performance can be ascribed to the excellent distribution of PVDF, superior adhesion to the active materials and to the substrate as well as improved electrical contact between active material particles and carbon black after heat treatment. This study demonstrates that introducing heat treatment to conventional PVDF-based electrode systems is critical to improving the performance of metal oxide electrodes undergoing drastic volume upon lithiation. Comprehensive evaluation of PVDF-based high-capacity metal oxide electrodes with heat treatment is thus highly meaningful and desirable for the development of high-performance LIBs.

Acknowledgements

The authors acknowledge funding support from the National Key Basic Research Program of China (973 Program, 2013CB934103), the National Natural Science Foundation of China (No. 21173054) and Science & Technology Commission of Shanghai Municipality (No. 08DZ2270500), China.

References

- [1] N. Recham, J.N. Chotard, L. Dupont, C. Delacourt, W. Walker, M. Armand, J.M. Tarascon, *Nat. Mater.* 9 (2010) 68–74.
- [2] K.S. Park, A. Benayad, D.J. Kang, S.G. Doo, *J. Am. Chem. Soc.* 130 (2008) 14930–14931.
- [3] K. Amine, I. Belharouak, Z.H. Chen, T. Tran, H. Yumoto, N. Ota, S.T. Myung, Y.K. Sun, *Adv. Mater.* 22 (2010) 3052–3057.
- [4] J.S. Chen, Y.L. Tan, C.M. Li, Y.L. Cheah, D.Y. Luan, S. Madhavi, F.Y.C. Boey, L.A. Archer, X.W. Lou, *J. Am. Chem. Soc.* 132 (2010) 6124–6130.
- [5] J. Liu, G.Z. Cao, Z.G. Yang, D.H. Wang, D. Dubois, X.D. Zhou, G.L. Graff, L.R. Pederson, J.G. Zhang, *ChemSusChem* 1 (2008) 676–697.
- [6] F. Wang, C.C. Lu, Y.F. Qin, C.C. Liang, M.S. Zhao, S.C. Yang, Z.B. Sun, X.P. Song, *J. Power Sources* 235 (2013) 67–73.
- [7] N. Yan, L. Hu, Y. Li, Y. Wang, H. Zhong, X.Y. Hu, X.K. Kong, Q.W. Chen, *J. Phys. Chem. C* 116 (2012) 7227–7235.
- [8] S. Yang, X. Feng, S. Ivanovici, K. Müllen, *Angew. Chem. Int. Ed.* 49 (2010) 8408–8411.
- [9] Y.G. Li, B. Tan, Y.Y. Wu, *Nano Lett.* 8 (2008) 265–270.
- [10] Y. Yao, J.J. Zhang, T. Huang, H. Mao, A.S. Yu, *Int. J. Electrochem. Sci.* 8 (2013) 3302–3309.
- [11] P. Poizot, S. Laruelle, S. Gruegeon, L. Dupont, J.M. Tarascon, *Nature* 407 (2000) 496–499.
- [12] X.W. Lou, D. Deng, J.Y. Lee, J. Feng, L.A. Archer, *Adv. Mater.* 20 (2008) 258–262.
- [13] K.T. Nam, D.W. Kim, P.J. Yoo, C.Y. Chiang, N. Meethong, P.T. Hammond, Y.M. Chiang, A.M. Belcher, *Science* 312 (2006) 885–888.
- [14] X.Y. Xue, S. Yuan, L.L. Xing, Z.H. Chen, B. He, Y.J. Chen, *Chem. Commun.* 47 (2011) 4718–4720.
- [15] J.M. Ma, A. Manthiram, *RSC Adv.* 2 (2012) 3187–3189.
- [16] Y. Wang, H. Xia, L. Lu, J. Lin, *ACS Nano* 4 (2010) 1425–1432.
- [17] A. Timmons, J.R. Dahn, *J. Electrochem. Soc.* 153 (2006) A1206–A1210.
- [18] Z. Chen, L. Christensen, J.R. Dahn, *Electrochem. Commun.* 5 (2003) 919–923.
- [19] Z. Chen, L. Christensen, J.R. Dahn, *J. Electrochem. Soc.* 150 (2003) A1073–A1078.
- [20] Z.Y. Wang, S. Madhavi, X.W. Lou, *J. Phys. Chem. C* 116 (2012) 12508–12513.
- [21] W.R. Liu, M.H. Yang, H.C. Wu, S.M. Chiao, N.L. Wu, *Electrochem. Solid State Lett.* 8 (2005) A100–A103.
- [22] J. Li, L. Christensen, M.N. Obrovac, K.C. Hewitt, J.R. Dahnc, *J. Electrochem. Soc.* 155 (2008) A234–A238.
- [23] C.Z. Yuan, X.G. Zhang, L.R. Hou, L.F. Shen, D.K. Li, F. Zhang, C.G. Fan, J.M. Li, *J. Mater. Chem.* 20 (2010) 10809–10816.
- [24] S. Vijayanand, R. Kannan, H.S. Potdar, V.K. Pillai, P.A. Joy, *J. Appl. Electrochem.* 43 (2013) 995–1003.
- [25] H. Huang, W.J. Zhu, X.Y. Tao, Y. Xia, Z.Y. Yu, J.W. Fang, Y.P. Gan, W.K. Zhang, *ACS Appl. Mater. Interfaces* 4 (2012) 5974–5980.
- [26] Q. Hao, M.H. Li, S.Z. Jia, X.Y. Zhao, C.X. Xu, *RSC Adv.* 3 (2013) 7850–7854.
- [27] Y. Wang, H.J. Zhang, J. Wei, C.C. Wong, J.Y. Lin, A. Borgna, *Energy Environ. Sci.* 4 (2011) 1845–1854.
- [28] J.S. Chen, T. Zhu, Q.H. Hu, J. Gao, F. Su, S.Z. Qiao, X.W. Lou, *ACS Appl. Mater. Interfaces* 2 (2010) 3628–3635.
- [29] G.P. Kim, I. Nam, N.D. Kim, J. Park, S. Park, J. Yi, *Electrochem. Commun.* 22 (2012) 93–96.
- [30] L. Li, K.H. Seng, Z.X. Chen, Z.P. Guo, H.K. Liua, *Nanoscale* 5 (2013) 1922–1928.
- [31] P. Malik, M. Castro, C. Carrot, *Polym. Degrad. Stab.* 91 (2006) 634–640.
- [32] K.J. Kim, Y. Doi, H. Abe, *Polym. Degrad. Stab.* 93 (2008) 776–785.
- [33] L.A. Riley, S.H. Leea, L. Gedvilasb, A.C. Dillonb, *J. Power Sources* 195 (2010) 588–592.
- [34] R. Xu, H.C. Zeng, *J. Phys. Chem. B* 107 (2003) 12643–12649.
- [35] S. Laruelle, S. Gruegeon, P. Poizot, M. Dolle, L. Dupont, J.M. Tarascon, *J. Electrochem. Soc.* 149 (2002) A627–A634.
- [36] L.P. Zhu, Z. Wen, W.M. Mei, Y.G. Li, Z.Z. Ye, *J. Phys. Chem. C* 117 (2013) 20465–20473.
- [37] J. Li, J.R. Dahn, *Electrochem. Solid State Lett.* 10 (2006) A17–A20.
- [38] D. Bevers, R. Rogers, M. von Bradke, *J. Power Sources* 63 (1996) 193–201.
- [39] G.R. Li, X. Feng, Y. Ding, S.H. Ye, X.P. Gao, *Electrochim. Acta* 78 (2012) 308–315.
- [40] H. Deng, I. Belharouak, C.S. Yoon, Y.K. Sun, K. Amine, *J. Electrochem. Soc.* 157 (2010) A1035–A1039.
- [41] H.Z. Zhang, Q.Q. Qiao, G.R. Li, S.H. Ye, X.P. Gao, *J. Mater. Chem.* 22 (2012) 13104–13109.